An Effective Spatial Modulation Based Scheme for Indoor VLC Systems

Shimaa Naser, Lina Bariah, *Senior Member, IEEE*, Sami Muhaidat, *Senior Member, IEEE*, Mahmoud Al-Qutayri, *Senior Member, IEEE*, and Paschalis C. Sofotasios, *Senior Member, IEEE*

***Abstract*—We propose an enhanced spatial modulation (SM)-based scheme for indoor visible light communication systems. This scheme enhances the achievable throughput of conventional SM schemes by transmitting higher order complex modulation symbol, which is decomposed into three different parts. These parts carry the amplitude, phase, and quadrant components of the complex symbol, which are then represented by unipolar pulse amplitude modulation (PAM) symbols. Superposition coding is exploited to allocate a fraction of the total power to each part before they are all multiplexed and transmitted simultaneously, exploiting the entire available bandwidth. At the receiver, a two-step decoding process is proposed to decode the active light emitting diode index before the complex symbol is retrieved. It is shown that at higher spectral efficiency values, the proposed modulation scheme outperforms conventional SM schemes with PAM symbols in terms of average symbol error rate (ASER), and hence, enhancing the system throughput. Furthermore, since the performance of the proposed modulation scheme is sensitive to the power allocation factors, we formulated an ASER optimization problem and propose a sub-optimal solution using successive convex programming (SCP). Notably, the proposed algorithm converges after only few iterations, whilst the performance with the optimized power allocation coefficients outperforms both random and fixed power allocation.**

***Index Terms*—Error rate, modulation, optimization, power allocation, visible light communications.**

I. Introduction

VISIBLE light communication (VLC) is envisioned to play a core role in future wireless networks as an efficient method to complement overcrowded radio frequency (RF) systems [1], [2]. Within this context, VLC utilizes the indoor light emitting diodes (LEDs) for both illumination and wireless data transmission [3]. It is worth mentioning that the intensity of the light emitted from the LEDs is modulated in order to transmit the corresponding information signal [4], [5]. This process is usually referred to as intensity modulation (IM). On the other hand, a photo detector (PD) is utilized at the receiver in order to retrieve the original signal, a process known as direct detection (DD). However, VLC systems suffer from the limited modulation bandwidth of LEDs in addition to the constraints imposed by IM/DD schemes that, unlike RF communications, require the transmitted signals to be positive and real-valued [6], [7]. Hence, the implementation of spectrally efficient modulation schemes that overcome these limitations is of paramount importance for the design of efficient high data rate VLC systems [5], [7]–[10].

Based on the above, extensive research efforts have been devoted in order to come up with high spectral efficiency modulation techniques. To that end, multiple-input multiple-output (MIMO) index modulation schemes have recently emerged as an efficient way to enhance the spectral and energy efficiency of wireless transmission through the activation states of the building blocks of communication systems [11]. Different investigations on spatial domain index modulation have been carried out in the context of VLC, such as space shift keying (SSK), generalized space shift keying (GSSK) and spatial modulation (SM), wherein, the transmitting LED index is used to transmit further information [12]–[16]. In addition, multiple active SM (MA-SM) has been proposed as a generalized version of SM which is capable of enhancing the achievable spectral efficiency by conveying more information in both spatial and signal domains [17]. The operation of MA-SM relies on the activation of N_a LEDs out of N_t with multiple distinct real non-negative M-ary symbols transmitted from each active LED. Yet, it is noted that despite the undoubted advantages of these schemes, their performance is highly affected by the incurred channel similarity associated with the nature of VLC channels.

Recent research efforts have focused on new techniques aiming to improve the performance of SM-based schemes in VLC systems. For instance, the authors in [17] and [18] modified the selection of symbols to be transmitted through the active LEDs based on collaborative constellation in order to improve the power efficiency of conventional SM schemes. Furthermore, the authors in [16] proposed an LED grouping scheme aiming

Manuscript received January 14, 2022; accepted January 17, 2022. Date of publication January 25, 2022; date of current version February 11, 2022. This work was supported by Khalifa University under Grants KU/FSU-8474000122 and KU/RC1-C2PS-T2/8474000137. (*Corresponding Author: Paschalis C. Sofotasios*.)

Shimaa Naser and Lina Bariah are with the Center for Cyber-Physical Systems, Department of Electrical Engineering and Computer Science, Khalifa University, Abu Dhabi 127788, UAE (e-mail: 100049402@ku.ac.ae; lina.bariah@ieee.org).

Sami Muhaidat is with the Center for Cyber-Physical Systems, Department of Electrical Engineering and Computer Science, Khalifa University, Abu Dhabi 127788, UAE, and also with the Department of Systems and Computer Engineering, Carleton University, Ottawa, ON K1S 5B6, Canada (e-mail: muhaidat@ieee.org).

Mahmoud Al-Qutayri is with the Systems-on-Chip Center, Department of Electrical Engineering and Computer Science, Khalifa University, Abu Dhabi 127788, UAE (e-mail: mahmoud.alqutayri@ku.ac.ae).

Paschalis C. Sofotasios is with the Center for Cyber-Physical Systems, Department of Electrical Engineering and Computer Science, Khalifa University, Abu Dhabi 127788, UAE, and also with the Department of Electrical Engineering, Tampere University, 33014 Tampere, Finland (e-mail: p.sofotasios@ieee.org).

Digital Object Identifier 10.1109/JPHOT.2022.3144656

This work is licensed under a Creative Commons Attribution 4.0 License. For more information, see https://creativecommons.org/licenses/by/4.0/

to improve the error rate performance of SM schemes. In particular, they considered that the LEDs are separated into different groups with the purpose of alleviating the channel correlation among each group. Within the same context, in [15], the authors proposed a receiver-oriented SM scheme to efficiently mitigate the optical channel correlation across the multiple LEDs. Additionally, in [19], the authors proposed an augmented SM scheme that allows each transmitter to have its own identity that is embedded in the transmitted signal and can only be decoded by the indented receiver. On the contrary, non-DC biased optical orthogonal frequency division multiplexing (OFDM) was combined with SM in [20]; however, it is rather common that OFDM suffers from the high peak-to-average power ratio, which has detrimental effects in OFDM-based VLC systems. The authors in [21] proposed channel-adapted SM schemes to find the optimal combinations of active LEDs under controlled inter-channel interference. Similar investigations on integrating adaptive modulation schemes with SM appeared also in [10], [22], [23]. Finally, in order to enhance the error rate performance of adaptive SM schemes, the authors of [7] proposed a flexible SM scheme that changes the modulation sizes over the LEDs and the number of active LEDs.

As already mentioned, the main challenge of using IM/DD schemes is the restrictions associated with the transmitted signals. Therefore, in order to transmit complex-valued symbols, different contributions investigated the design of multiple-LED complex modulation schemes, including quad-LED and dual-LED complex modulation. For instance, the authors in [24] proposed a complex modulation scheme called quad-LED complex modulation (QCM) for MIMO VLC systems. In this scheme, the spatial domain was utilized to transmit the real and imaginary parts of the complex-valued symbols. Similarly, [25] discussed the integration of QCM and SM to further enhance the achievable transmission rate. Furthermore, the authors in [26] proposed two complex modulation schemes called quadrature spatial modulation (QSM) and dual mode index modulation (DMIM) with a dual-LED complex modulator (DCM). Nevertheless, the use of quad-LED and dual-LED complex modulations results in spectral efficiency loss when combined with SM since part of complex signal is carried over the spatial domain. Additionally the associated computational complexity with these two schemes is rather high.

Based on above, the available contributions on the performance enhancement of SM have been based on two main approaches: i) Employing multiple active LEDs with LED selection optimization and the use of complicated adaptive schemes in order to achieve a balance between error rate and spectral efficiency performance. ii) Using quad-LED and dual-LED. However, the latter approach yields an increased system complexity and limits the spectral efficiency when integrated with SM-based techniques because part of the complex symbol is conveyed through the spatial domain. Hence, in the current contribution, we aim to design an efficient higher order SM-based modulation scheme that can achieve an adequate balance between error rate performance and spectral efficiency, while maintaining a relatively reduced involved implementation complexity.

With this motivation, in order to improve the performance of conventional SM schemes, we propose the transmission of a superimposed signal of the amplitude, phase, and quadrant components over the signal domain and provide a formulation of the associated power allocation optimization. To the best of our knowledge, such a contribution is novel, and has not been considered previously in the open literature. More specifically, in order to transmit a complex-valued symbol, the signal domain information is decomposed into three different parts that are used to carry the amplitude, phase, and quadrant components. Then, each component is represented by a unipolar pulse-amplitude modulation (PAM) signal. Subsequently, superposition coding is exploited to allocate each part a certain fraction of the total power. Then, all parts are multiplexed and transmitted at the same time, exploiting the entire available bandwidth. To this effect and given that power allocation is an essential factor that determines the overall system error performance, we also formulate an average symbol error rate (ASER) minimization constrained optimization problem in order to find the optimum power allocation coefficients for each signal part. Then, the formulated non-convex optimization problem is effectively and sub-optimally solved using successive convex programming (SCP) with trust region algorithm.

In summary, the main contributions of the present work are listed below:

- We propose a novel SM-based scheme, so called APQ-SM, that transmits complex-valued APQ symbols from the active LED.
- We derive closed form expressions for the ASER for both joint and two-step detection. These expressions have a relatively simple algebraic representation which renders them tractable both analytically and numerically.
- Capitalizing on the above, we quantify the achievable ASER performance of the proposed scheme for both joint detection and the proposed two-step detection process, which leads to the development of useful theoretical and practical insights.
- An efficient power allocation scheme for each part of the APQ symbol is proposed, where we formulate a constrained optimization problem for finding the optimum power allocation coefficients that minimize the ASER. Then, we propose an effective sub-optimal solution to the formulated non-convex optimization problem using SCP with trust region algorithm.
- Extensive Monte Carlo simulations are carried out in order to validate the derived analytic expressions and to demonstrate the ASER performance under different spectral efficiency levels and LEDs separations.

The remainder of the paper is organized as follows: Section II describes the channel and system model of the proposed APQ-SM based VLC downlink network. Section III presents the proposed decoding process, the derivation of the analytic expressions for the corresponding ASER, and the formulation of the optimization problem. Numerical results and useful related discussions are presented in Section IV, whereas closing remarks are provided in Section V.

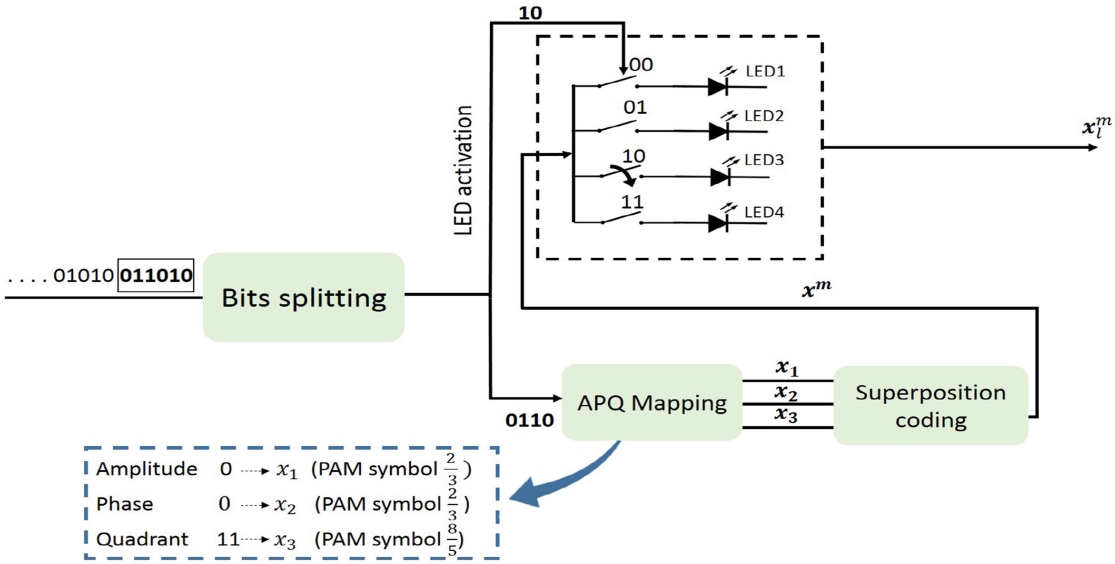

Fig. 1. APQ-SM transmitter.

Notations: Throughout the paper, and unless otherwise stated, boldface uppercase and lowercase represent matrices and vectors, respectively, whereas $(\cdot)^T$ denotes the transpose operation. Moreover, $||\cdot||$ denotes the Euclidean norm and $|\cdot|$ represents the absolute value. Also, $\text{tr}(\mathbf{A})$ denotes the trace of a matrix $\mathbf{A}$, while $\text{diag}(\mathbf{x})$ is a diagonal matrix whose entries are the vector $\mathbf{x}$. Finally, $\mathbf{0}$ accounts for the all-zeros vector.

II. System and Channel Models

We consider an indoor VLC MIMO downlink system which consists of N_t transmit LEDs, assumed to be power of 2, and a user with N_r PDs. Also, and without loss of generality, the dimensions of the room are considered to be $3\ m \times 3\ m \times 3\ m$. To this effect, the transmitted bit stream is divided into two parts: i) the first part consists of $\log_2(N_t)$ bits, which are used to select the index of the active LED; ii) the second part consists of the other $\log_2(M)$ bits, which are modulated using M-ary APQ modulation. The considered APQ-SM transmitter is illustrated in detail in Fig. 1.

Based on the above, in order to construct the m^{th} symbol in M-ary APQ modulation, the $\log_2(M)$ bits are divided into three different parts, namely, the amplitude, phase, and quadrant components. Then, each component is modulated using an M_i-ary PAM, as follows:

$$x_i^m \in \left\{ \frac{2}{M_i+1}, \frac{4}{M_i+1}, \ldots, \frac{2\,M_i}{M_i+1} \right\}, \quad i = 1, 2, 3. \tag{1}$$

It is worth noting that the symbols in (1) are chosen in order to maintain a fixed average optical power, and hence, fixed illumination in the room. Subsequently, all components are superimposed in power domain and are transmitted simultaneously to fit with the constraints imposed by the nature of VLC systems. Therefore, the m^{th} APQ symbol x^m can be represented as [9]

$$x^m = p_1 x_1^m + p_2 x_2^m + p_3 x_3^m, \tag{2}$$

where p_1, p_2, and p_3 represent the optical power allocation for each component. It is worth noting that we assumed that

$$\sum_{i=1}^{3} p_i = P_{\text{opt}}, \tag{3}$$

and $p_i < p_{i-1},\ i = 2, 3$, where P_{opt} denotes the mean optical power of the corresponding LED. Based on this, the average symbol energy, E_s, can be expressed as follows:

$$E_s = \gamma^2 P_{\text{opt}}^2\, T_s, \tag{4}$$

where γ represents the optical-to-electrical conversion factor, and T_s denotes the symbol duration.

The concept of the proposed modulation scheme is demonstrated in more detail in Fig. 1. This represents an APQ-SM system with an indicative spectral efficiency of $\eta = 6$ bpcu, which is realized by having 4 LEDs at the transmitter side in order to transmit 2 bits in the spatial domain and 4 bits for the 16-APQ symbol. Then, the 16-APQ symbol is constructed as follows: the 4 bits are divided into three parts; the first bit is used to represent one of the two amplitudes (i.e., L_1, L_2) through 2-PAM modulation, the next two bits represent the four quadrant through 4-PAM modulation, and the last bit is used to represent the two phases (i.e., θ_1, θ_2) through 2-PAM modulation. Then, each resulted PAM symbol is allocated a fraction of the total power and finally they are superimposed and transmitted from the active LED.

Based on the above, the received information signal can be expressed as follows:

$$\mathbf{y} = \gamma \mathbf{H} \mathbf{x}_\ell^m + \mathbf{z}, \tag{5}$$

where $\mathbf{x}_\ell^m$ is the m^{th} APQ symbol transmitted from the ℓ^{th} LED, which is represented as

$$\mathbf{x}_\ell^m = [0, \ldots, 0, x^m, 0, \ldots, 0]. \tag{6}$$

Moreover, $\mathbf{z}$ represents the additive white Gaussian noise (AWGN) vector, where each component has zero mean and variance $\sigma^2 = N_0 B$, with N_0 denoting the noise power spectral density and B the channel bandwidth [27]. Additionally, $\mathbf{H}_{N_r \times N_t}$ denotes the channel gain matrix between the LEDs and the PDs, in which only the line-of-sight (LoS) components are considered. Based on this, each component of $\mathbf{H}$ can be expressed as [28]

$$h_{r\ell} = \begin{cases} \frac{A}{d_{r\ell}^2} R_o(\varphi_{r\ell}) T_s(\phi_{r\ell}) g(\phi_{r\ell}) \cos(\phi_{r\ell}), & 0 \leqslant \phi_{r\ell} \leqslant \phi_c, \\ 0, & \text{otherwise}, \end{cases} \tag{7}$$

where A denotes the PD area, $d_{r\ell}$ is the distance between the ℓ^{th} LED and the r^{th} PD, $\varphi_{r\ell}$ is the angle of transmission from the ℓ^{th} LED to the r^{th} PD, $\phi_{r\ell}$ is the incident angle with respect to the receiver, and ϕ_c is the field of view (FoV) of the PD. Furthermore, $T_s(\phi_{r\ell})$ and $g(\phi_{r\ell})$ denote the gains of the optical filter and concentrator, respectively, whereas $g(\phi_{r\ell})$ can be expressed as follows:

$$g(\phi_{r\ell}) = \begin{cases} \frac{n^2}{\sin^2(\phi_c)}, & 0 \leqslant \phi_{r\ell} \leqslant \phi_c, \\ 0, & \phi_{r\ell} > \phi_c. \end{cases} \tag{8}$$

In the above, n represents the corresponding refractive index, and $R_o(\varphi_{r\ell})$ denotes the Lambertian radiant intensity, namely

$$R_o(\varphi_{r\ell}) = \frac{\nu + 1}{2\pi} \left(\cos(\varphi_{r\ell})\right)^{\nu}, \tag{9}$$

with ν representing the order of the Lambertian emission, which is expressed as

$$\nu = \frac{-\ln(2)}{\ln\left(\cos(\varphi_{1/2})\right)}, \tag{10}$$

given that $\varphi_{1/2}$ is the LED semi-angle at half power [29].

III. Proposed ML Decoding

Following from the above, this section is devoted in the quantification of the performance of the proposed system model by means of analyzing the achievable symbol error rate performance. To this end, assuming maximum likelihood (ML) detection is utilized at the receiver side, the detector performs joint detection to deduce the received signals over the space and signal domains. In particular, the receiver detects jointly the LED index and the transmitted APQ symbol according to the following criterion:

$$\mathbf{x}_{\hat{\ell}}^{\hat{m}} = \arg \min_{\forall \mathbf{x}_{\tilde{\ell}}^{\tilde{m}} \in \chi} \left\| \mathbf{y} - \gamma \mathbf{H} \mathbf{x}_{\tilde{\ell}}^{\tilde{m}} \right\|^2, \tag{11}$$

where $\mathbf{x}_{\hat{\ell}}^{\hat{m}}$ is the estimated APQ-SM symbol that minimizes the distance between the received signal and all potential APQ-SM symbols. It is recalled here that joint ML detection requires the search over all $M \times N_t$ combinations of the indices and symbols, which results in an increased receiver complexity. Therefore, the upper bound on the achievable SER using joint detection, $P_{e,\text{joint}}$, is expressed as

$$P_{e,\text{joint}} \leqslant \frac{1}{N_t\, M} \sum_{\forall (m,\ell)} \sum_{\substack{\forall (\hat{m},\hat{\ell}) \\ \neq \\ (m,\ell)}} Q\left(\sqrt{\frac{\gamma^2}{4\sigma^2} \left\| \mathbf{H}(\mathbf{x}_{\ell}^{m} - \mathbf{x}_{\hat{\ell}}^{\hat{m}}) \right\|^2} \right), \tag{12}$$

where $Q(\cdot)$ denotes the one dimensional Gaussian $Q-$function [30]. As already mentioned, it is of paramount importance to achieve a reduced complexity receiver in the considered VLC system. To that end, we propose a new detection mechanism in which the detection process is performed over two stages. Hence, this yields a reduced complexity in terms of number of iterations, i.e., the search space is reduced to $M + \lfloor \binom{N_t}{1} \rfloor_{2^p}$. The first stage comprises a conditional ML detection, in which, conditioned on $\mathbf{x}_{\tilde{\ell}}^{m}$, the receiver detects only the index of the transmitting LED, namely

$$\hat{\ell} = \arg \min_{\forall \tilde{\ell}} \left(\min_{\forall m} \left\| \left[\left(\mathbf{y} - \gamma \mathbf{H} \mathbf{x}_{\tilde{\ell}}^{m} \right) | \mathbf{x}_{\tilde{\ell}}^{m} \right] \right\|^2 \right). \tag{13}$$

Then, in the second stage the receiver uses the detected index in order to detect the transmitted symbols. To this effect and assuming perfect detection of the ℓ^{th} LED index, the estimated symbol can be evaluated as follows:

$$\mathbf{x}_{\ell}^{\hat{m}} = \arg \min_{\forall \tilde{m}} \left\| \mathbf{y} - \gamma \mathbf{H}\, \mathbf{x}_{\ell}^{\tilde{m}} \right\|^2. \tag{14}$$

Capitalizing on the above, the next section is devoted in the evaluation of the achievable ASER performance of the proposed receiver.

A. Average SER Analysis

The probability of incorrect detection given that the ℓ^{th} LED is selected can be determined by

$$P_e^{\ell} = P_x(\mathbf{x}_{\ell}^{m} | \ell \neq \hat{\ell}).P_{\ell} + P_x(\mathbf{x}_{\ell}^{m} | \ell = \hat{\ell}).(1 - P_{\ell}), \tag{15}$$

where P_{ℓ} is probability of incorrect index detection, whereas $P_x(\mathbf{x}_{\ell}^{m} | \ell = \hat{\ell})$ and $P_x(\mathbf{x}_{\ell}^{m} | \ell \neq \hat{\ell})$ denote the probability of incorrect symbol detection conditioned on correct and incorrect index detection, respectively. Due to mathematical intractability of (15) and given that $P_x(\mathbf{x}_{\ell}^{m} | \ell \neq \hat{\ell})$ is rather large, close to unity, the error probability for the ℓ^{th} combination can be accurately simplified to the following

$$P_e^{\ell} \leqslant P_{\ell} + P_x(\mathbf{x}_{\ell}^{m} | \ell = \hat{\ell}).(1 - P_{\ell}). \tag{16}$$

Therefore, it is evident that the ASER can be obtained from (16) subject to analytic derivation of two explicit expressions, for P_{ℓ} and $P_x(\mathbf{x}_{\ell}^{m} | \ell = \hat{\ell})$ and subsequent averaging over all possible LEDs activation. Based on this, the following closed form expression for the ASER for P_{ℓ} is obtained

$$P_{\ell} = \frac{1}{M} \sum_{\forall m} Q\left(\sqrt{\frac{\gamma^2}{4\sigma^2} D^2(\mathbf{x}_{\ell}^{m})} \right), \tag{17}$$

where $D(\mathbf{x}_{\ell}^{m})$ is the minimum distance between the symbol $\mathbf{x}_{\ell}^{m}$ transmitted from the ℓ^{th} LED index and all possible symbols

that can be transmitted from all other LEDs, namely

$$D(\mathbf{x}_\ell^m) = \min_{\substack{\forall \hat{\ell}, \ell \neq \hat{\ell} \\ \forall \hat{m}}} \left\| \gamma \mathbf{H}(\mathbf{x}_\ell^m - \mathbf{x}_{\hat{\ell}}^{\hat{m}}) \right\|. \tag{18}$$

Based on this and utilizing the union bound on the SER, we evaluate the probability of incorrectly detecting the symbol, $P_x(\mathbf{x}_\ell^m | \ell = \hat{\ell})$, as follows:

$$P_x(\mathbf{x}_\ell^m | \ell = \hat{\ell}) = \frac{1}{M} \sum_{\forall m} \sum_{\substack{\forall \hat{m} \\ m \neq \hat{m}}} P(\mathbf{x}_\ell^m \longrightarrow \mathbf{x}_\ell^{\hat{m}}), \tag{19}$$

where $P(\mathbf{x}_\ell^m \longrightarrow \mathbf{x}_\ell^{\hat{m}})$ denotes the pairwise error probability (PEP) of decoding $\mathbf{x}_\ell^m$ as $\mathbf{x}_\ell^{\hat{m}}$, which is represented as

$$P(\mathbf{x}_\ell^m \longrightarrow \mathbf{x}_\ell^{\hat{m}}) = Q\left(\sqrt{\frac{\gamma^2}{4\sigma^2} \left\| \mathbf{H}(\mathbf{x}_\ell^m - \mathbf{x}_\ell^{\hat{m}}) \right\|^2} \right). \tag{20}$$

Therefore, by substituting (20) in (19), the ASER for incorrectly detecting the symbol $P_x(\mathbf{x}_\ell^m | \ell = \hat{\ell})$ is given by the following analytic expression

$$P_x(\mathbf{x}_\ell^m | \ell = \hat{\ell}) = \frac{1}{M} \sum_{\forall m} \sum_{\substack{\forall \hat{m} \\ m \neq \hat{m}}} Q\left(\sqrt{\frac{\gamma^2}{4\sigma^2} \left\| \mathbf{H}(\mathbf{x}_\ell^m - \mathbf{x}_\ell^{\hat{m}}) \right\|^2} \right). \tag{21}$$

Finally, using (16), (17) and (21) and averaging over all possible LEDs activation, the total upper bound on the corresponding SER can be expressed according to (22), shown at the bottom of the page.

To the best of the authors' knowledge, the offered analytic results have not been previously reported in the open technical literature. In what follows, these results are employed in the determination of effective power allocation strategies in the considered APQ-SM based VLC system.

B. Power Allocation Optimization

It is recalled that the performance of the proposed scheme is largely dependent upon the factors relating to the corresponding power allocation strategy. Based on this, in this section we formulate an optimization problem that aims to minimize the ASER obtained from the performed joint detection. To that end, we first expand the norm to represent $P_{e,joint}$ in (12) in terms of the p_i parameters in (23), shown at the bottom of the page, which can be further simplified as (24), shown at the bottom of the page, where

$$\Delta_i^r(m, \ell, \hat{m}, \hat{\ell}) = x_i^{\hat{m}} h_{r\hat{\ell}} - x_i^m h_{r\ell}, \tag{25}$$

with $i = 1, 2, 3$ and $r = 1, \ldots, N_r$. To this effect and assuming a predetermined spectral efficiency, we formulate the following minimization problem:

$$\min_{\mathbf{p}} \quad \frac{1}{N_t\, M} \sum_{\forall \ell} \sum_{\forall m} \sum_{\forall \hat{\ell}} \sum_{\forall \hat{m}} Q\left(\frac{\gamma}{2\sigma} \sqrt{\sum_{r=1}^{N_r} \left| \mathbf{p}^T \boldsymbol{\Delta}^r(m, \ell, \hat{m}, \hat{\ell}) \right|^2} \right) \tag{P1}$$

$$\text{s.t.} \quad \text{tr}(\text{diag}(\mathbf{p})) = P_{opt}, \tag{P1.a}$$

$$\mathbf{p} \geq \mathbf{0}, \tag{P1.b}$$

$$p_i \leqslant p_{(i-1)}, \quad i = 2, 3, \tag{P1.c}$$

where $\boldsymbol{\Delta}^r(m,\ell,\hat{m},\hat{\ell}) = [\Delta_1^r(m,\ell,\hat{m},\hat{\ell}), \Delta_2^r(m,\ell,\hat{m},\hat{\ell}), \Delta_3^r(m,\ell,\hat{m},\hat{\ell})]$, whilst $\mathbf{p} = [p_1, p_2, p_3]^T$ denotes the power allocation vector. It is noted here that the optimization problem in (P1) is non-convex due

$$P_e \leqslant \frac{1}{N_t} \sum_{\forall \ell} \left[\frac{1}{M} \sum_{\forall m} Q\left(\sqrt{\frac{\gamma^2}{4\sigma^2} D^2(\mathbf{x}_\ell^m)} \right) + \frac{1}{M} \sum_{\forall m} \sum_{\substack{\forall \hat{m} \\ m \neq \hat{m}}} Q\left(\sqrt{\frac{\gamma^2}{4\sigma^2} \left\| \mathbf{H}(\mathbf{x}_\ell^m - \mathbf{x}_\ell^{\hat{m}}) \right\|^2} \right) \right.$$
$$\left. - \frac{1}{M} \sum_{\forall m} Q\left(\sqrt{\frac{\gamma^2}{4\sigma^2} D^2(\mathbf{x}_\ell^m)} \right) \times \frac{1}{M} \sum_{\forall m} \sum_{\substack{\forall \hat{m} \\ m \neq \hat{m}}} Q\left(\sqrt{\frac{\gamma^2}{4\sigma^2} \left\| \mathbf{H}(\mathbf{x}_\ell^m - \mathbf{x}_\ell^{\hat{m}}) \right\|^2} \right) \right]. \tag{22}$$

$$P_{e,\text{joint}} \leqslant \frac{1}{N_t\, M} \sum_{\forall \ell} \sum_{\forall m} \sum_{\forall \hat{\ell}} \sum_{\forall \hat{m}} Q\left(\frac{\gamma}{2\sigma} \sqrt{\sum_{r=1}^{N_r} \left| \left([p_1 x_1^{\hat{m}} + p_2 x_2^{\hat{m}} + p_3 x_3^{\hat{m}}] h_{r\hat{\ell}} \right) - \left([p_1 x_1^m + p_2 x_2^m + p_3 x_3^m] h_{r\ell} \right) \right|^2} \right), \quad (m, \ell) \neq (\hat{m}, \hat{\ell}). \tag{23}$$

$$P_{e,\text{joint}} \leqslant \frac{1}{N_t\, M} \sum_{\forall \ell} \sum_{\forall m} \sum_{\forall \hat{\ell}} \sum_{\forall \hat{m}} Q\left(\frac{\gamma}{2\sigma} \sqrt{\sum_{r=1}^{N_r} \left| p_1 \Delta_1^r(m, \ell, \hat{m}, \hat{\ell}) + p_2 \Delta_2^r(m, \ell, \hat{m}, \hat{\ell}) + p_3 \Delta_3^r(m, \ell, \hat{m}, \hat{\ell}) \right|^2} \right), \; (m, \ell) \neq (\hat{m}, \hat{\ell}) \tag{24}$$

to the non-convexity of the objective function in $\mathbf{p}$. In what follows, we propose an effective sub-optimum solution to this problem with the aid of SCP algorithm, due to its simplicity and high efficiency [31], [32]. To that end, we re-describe the algorithm by first noting that SCP solves a non-convex problem by repeatedly constructing a convex approximation to the problem around the current iterate $\mathbf{p}^{(l)}$. The sub-problem is then used to generate the new value of $\mathbf{p}^{(l+1)}$ that will be used in the next iteration. Based on this, there are different choices for the approximation function, namely: first-order Taylor series, second-order Taylor series with positive semi-definite Hessian, inner convex approximation, or any other convex function that locally approximates the non-convex objective function at $\mathbf{p}^{(l)}$. In the present analysis, the objective function is replaced by its first order Taylor series expansion at each iteration l around the point $\mathbf{p}^{(l)}$. However, the convergence and the accuracy of the approximation are particularly sensitive to the $||\mathbf{p}-\mathbf{p}^{(l)}||$ term. Hence, we incorporate the trust region method to control the step size which is reliable and robust, whilst it also exhibits adequate convergence properties. Based on this, it follows that (P1) can be approximated at iteration l by the following linear sub-problem:

$$\min_{\mathbf{p}} \quad E^{(l)} \tag{P2}$$

$$\text{s.t.} \quad \text{tr}(\text{diag}(\mathbf{p})) = P_{opt}, \tag{P2.a}$$

$$\mathbf{p} \geq \mathbf{0}, \tag{P2.b}$$

$$p_i \leqslant p_{(i-1)}, \quad i = 2, 3, \tag{P2.c}$$

$$||\mathbf{p}-\mathbf{p}^{(l)}|| \leqslant \delta^{(l)}, \tag{P2.d}$$

where the constraint in (P2.d) is used to define the trust region and $\delta^{(l)}$ is the iteration-based trust region radius [33], [34]. Additionally, $E^{(l)}$ is the first-order Taylor approximation at the l^{th} iteration, which is expressed as

$$E^{(l)} = (\mathbf{A}^{(l)})^T(\mathbf{p}-\mathbf{p}^{(l)}) + B^{(l)}, \tag{28}$$

where $\mathbf{A}^{(l)}$ and $\mathbf{B}^{(l)}$ are given by the explicit expressions in equations (29) and (30), shown at the bottom of the page.

It is recalled here that in trust region method, the new iteration is generated within a close region around the current point. Then, the radius of this region is adjusted according to an indicator function that determines how accurately the approximate model fits the original problem. Based on this, in order to decide on the value of $\delta^{(l+1)}$, we utilize the merit function for the actual problem displayed in (31) at the bottom of the page along with the following merit function for the approximated sub-problem

$$f_p(\mathbf{p}) = E^{(l)}. \tag{32}$$

To this effect and in order to decide on the value of $\delta^{(l+1)}$, the following relative performance metric is utilized

$$r^{(l)} = \frac{f_a(\mathbf{p}^l) - f_a(\mathbf{p}^{l+1})}{f_p(\mathbf{p}^l) - f_p(\mathbf{p}^{l+1})}. \tag{33}$$

Therefore, based on the value of $r^{(l)}$ the radius of the trust region is either, increased, decreased, or maintained unchanged. Additionally, the value of $r^{(l)}$ assists in deciding on whether to accept or reject the estimated point as a reference in the next iteration. Importantly, a common approach on this is to define three real numbers, $\alpha_0 < \alpha_1 < \alpha_2 \in (0,1)$, that split the range of the possible values of $r^{(l)}$ into four segments. Then, the value of the trust region radius and the reference point for the next iteration are updated according to the rule in the pseudo-code for the SCP detailed in Algorithm 1, where the parameters $\alpha, \beta > 0$ are user selected values and ϵ denotes the termination tolerance.

In Algorithm 1, the complexity of the power allocation is mainly associated with the SCP algorithm which is determined by the number of iterations that are required for convergence as well as the complexity for each iteration. Note that the number of iterations required by SCP is $\mathcal{O}(\sqrt{N_1}\,\log_2(1/\epsilon))$, where ϵ is the accuracy of SCP and N_1 is the number of constraints which is $2K-1$; here K denotes the number of variables in (P2). At each iteration, (P2) is solved with complexity of $\mathcal{O}(N_1\ K^2)$ [35]. Therefore, the overall complexity associated with the SCP is $\mathcal{O}(K^{1.5}\ \log_2(1/\epsilon))$, which means that the sub-optimal solution is computed in a polynomial time [36], [37].

It is noted here that evaluating the SER performance with respect to the average received electrical signal-to-noise ratio

$$\mathbf{A}^{(l)} = \frac{-\gamma}{\sigma N_t\ M\ \sqrt{8\pi}} \sum_{\forall \ell} \sum_{\forall m} \sum_{\forall \hat{\ell}} \sum_{\forall \hat{m}} e^{-\frac{1}{2}\left(\frac{\gamma^2}{4\sigma^2}\sum_{r=1}^{N_r}\left|(\mathbf{p}^{(l)})^T\mathbf{\Delta}^r(m,\ell,\hat{m},\hat{\ell})\right|^2\right)} \frac{\sum_{r=1}^{N_r}\left((\mathbf{p}^{(l)})^T\mathbf{\Delta}^r(m,\ell,\hat{m},\hat{\ell})\right)\mathbf{\Delta}^r(m,\ell,\hat{m},\hat{\ell})}{\sqrt{\sum_{r=1}^{N_r}\left|(\mathbf{p}^{(l)})^T\mathbf{\Delta}^r(m,\ell,\hat{m},\hat{\ell})\right|^2}} \tag{29}$$

$$B^{(l)} = \frac{1}{N_t\ M} \sum_{\forall \ell} \sum_{\forall m} \sum_{\forall \hat{\ell}} \sum_{\forall \hat{m}} Q\left(\frac{\gamma}{2\sigma}\sqrt{\sum_{r=1}^{N_r}\left|(\mathbf{p}^{(l)})^T\mathbf{\Delta}^r(m,\ell,\hat{m},\hat{\ell})\right|^2}\right) \tag{30}$$

$$f_a(\mathbf{p}) = \frac{1}{N_t\ M} \sum_{\forall \ell} \sum_{\forall m} \sum_{\forall \hat{\ell}} \sum_{\forall \hat{m}} Q\left(\frac{\gamma}{2\sigma}\sqrt{\sum_{r=1}^{N_r}\left|\mathbf{p}^T\mathbf{\Delta}^r(m,\ell,\hat{m},\hat{\ell})\right|^2}\right) \tag{31}$$

Algorithm 1: SCP Algorithm with Trust Region Approach.

Initialization: set $\mathbf{p}^{(0)}$,$\delta^{(0)}$, $\alpha_0, \alpha_1, \alpha_2, \alpha, \beta$, and tolerance ϵ

for l = *0 until meeting termination condition* **do**

- Obtain $\mathbf{p}^{(l+1)}$ by solving (P2) using $\mathbf{p}^{(l)}$:
- **if** $|\mathbf{p}^{(l+1)} - \mathbf{p}^{(l)}| \leq \epsilon$, *or* N_{max} *is reached* **then**
  - Break;
- **else**
  - **if** $r^{(l)} \geq \alpha_2$ **then**
    - $\delta^{(l+1)} = \beta\delta^{(l)}$, and accept $\mathbf{p}^{(l+1)}$
  - **if** $\alpha_1 \leqslant r^{(l)} < \alpha_2$ **then**
    - $\delta^{(l+1)} = \delta^{(l)}$, and accept $\mathbf{p}^{(l+1)}$
  - **if** $\alpha_0 \leqslant r^{(l)} < \alpha_1$ **then**
    - $\delta^{(l+1)} = \delta^{(l)}/\alpha$, and accept $\mathbf{p}^{(l+1)}$
  - **if** $r^{(l)} < \alpha_0$ **then**
    - $\delta^{(l+1)} = \delta^{(l)}/\alpha$, and reject $\mathbf{p}^{(l+1)}$, $\mathbf{p}^{(l)}$ is retained
- Set $l = l + 1$

(SNR) would disregard the individual path loss of different setups and the particular activated LED. Therefore, in order to provide a more fair comparison, we evaluate the SER performance of the proposed scheme with respect to the transmit SNR, which is defined as the ratio of the average symbol energy against the noise power spectral density E_s/N_0 [38], [39]. It is also emphasized that the value of E_s/N_0 in VLC systems is considerably greater than that of counterpart RF systems [40], [41]. This difference is attributed to the small value associated with the noise power spectral density N_0 [42]. More specifically, by neglecting the photodetector dark current, the N_0 term is expressed as $N_0 \simeq q\, I_B$, where $q = 1.6e{-}19$ is the charge of electron and I_B denotes the involved background noise current that typically takes values in the order of μA [27], [43] and the references therein.

IV. Numerical Results and Insights

In what follows, we exploit the offered results in the previous sections to quantify the achievable ASER of the proposed modulation scheme in the considered VLC setup. The presented analytic representations are thoroughly corroborated by extensive results from respective Monte Carlo simulations, which justify the validity of the analytic derivations and the proposed SCP based suboptimum algorithm for the corresponding power allocation. The obtained analytic and simulation results are subsequently compared with respective results corresponding to the conventional SM with PAM scheme as well as to the MA-SM scheme. Without loss of generality, these analyses and comparisons are carried out for the case of an indoor environment with dimensions $3\ m \times 3\ m \times 3\ m$, which includes $N_t = 4$ high brightness white LEDs attached to the ceiling at a height of $2.5\ m$ and with a d_{TX} separation distance between them. Additionally, we assume that the receiver has $N_r = 4$ PDs placed at a height of $0.75\ m$. All parameters used in the simulation as well as the LEDs and PDs locations are summarized in Tables I and II, respectively.

TABLE I
Simulation Parameters

Parameter	Symbol	Value
Room dimensions	-	$3\ m \times 3\ m \times 3\ m$
LED beam angle	$\varphi_{1/2}$	15^o
PD area	A	$1\ cm^2$
Gain of optical filter	$T_s(\phi_{r\ell})$	1
FoV of PD	ϕ_c	15^o
Optical-to-electrical conversion factor	γ	$1\ A/W$
LED optical power	P_{opt}	$1\ W$

TABLE II
LEDs and PDs Locations

LEDs locations ($d_{TX} = 0.2\ m$)	PDs locations
LED 1: [1.6 1.6 2.5]	PD 1: [1.55 1.55 0.75]
LED 2: [1.4 1.6 2.5]	PD 2: [1.45 1.55 0.75]
LED 3: [1.6 1.4 2.5]	PD 3: [1.55 1.45 0.75]
LED 4: [1.4 1.4 2.5]	PD 4: [1.45 1.45 0.75]

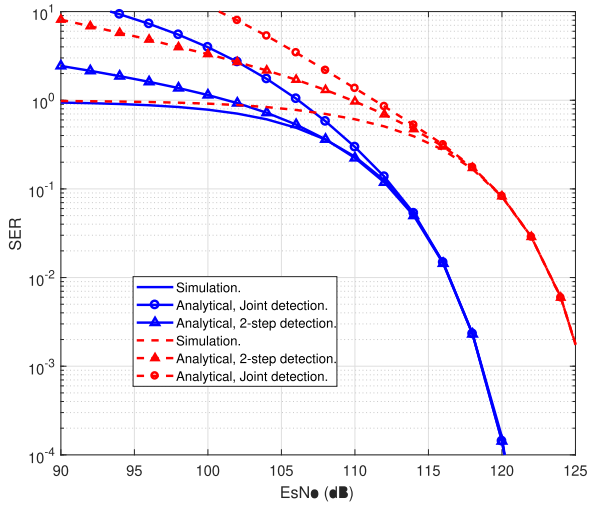

Fig. 2. Comparison between the two-step and joint detection methods. Solid lines correspond to $\eta = 6$ bpcu, whereas dashed lines correspond to $\eta = 8$ bpcu.

Based on the above, we first validate the derived analytic expressions for the upper bound on the ASER in Section III. Fig. 2 illustrates the analytical and Monte Carlo results for the SER with regard to the transmit SNR for two different spectral efficiency values, namely $\eta = 6$ bpcu and $\eta = 8$ bpcu. It is clearly observed that the proposed upper bounds are particularly tight from moderate SNR values to the high SNR regime with respect to the corresponding Monte Carlo simulation. It is also noticed that since the channel gains are in the order of 10^{-4}, the received SNR will experience an about 80dB shift with respect to the transmit SNR, which corresponds to the typical values in VLC systems. In addition, it can be noticed that the two-step

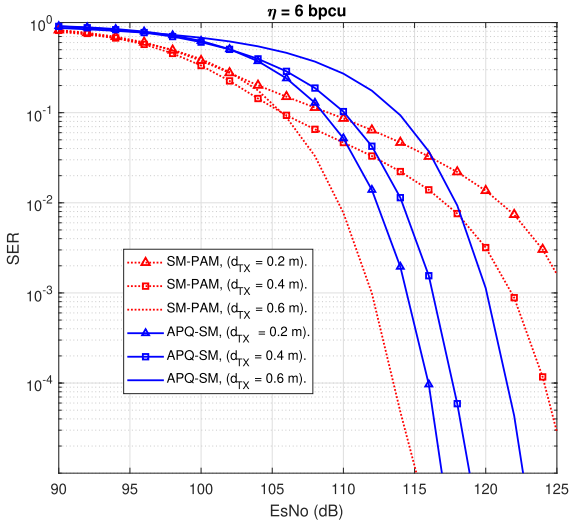

Fig. 3. Comparison between APQ-SM and SM-PAM in [38] for spectral efficiency 6 bpcu.

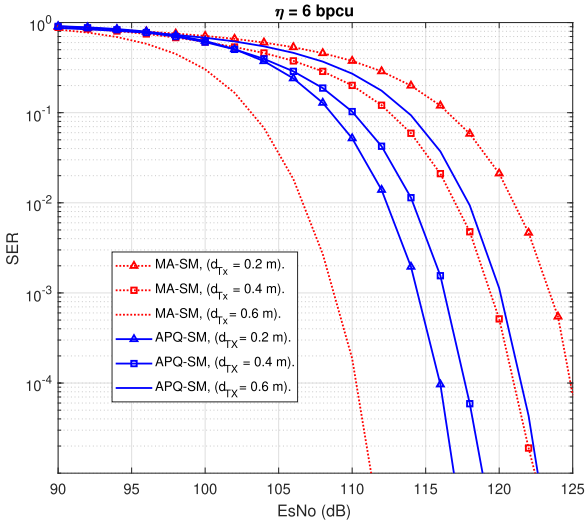

Fig. 5. Comparison between APQ-SM and MA-SM in [44] for spectral efficiency 6 bpcu.

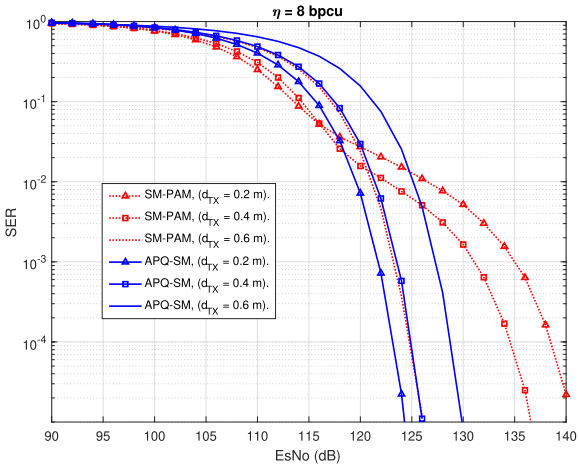

Fig. 4. Comparison between APQ-SM and SM-PAM in [38] for spectral efficiency 8 bpcu.

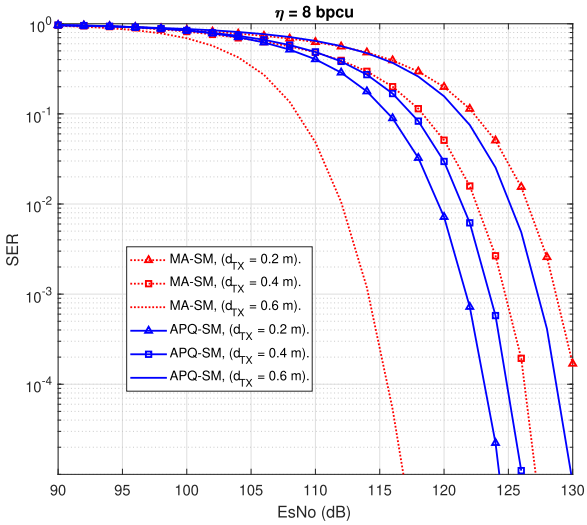

Fig. 6. Comparison between APQ-SM and MA-SM in [44] for spectral efficiency 8 bpcu.

detection process is tighter at the low SNR regime, which is in fact because the detection is performed in two stages.

Next, we examine the SER performance of the proposed modulation scheme and compare it with the SM-PAM scheme. Fig. 3 and Fig. 4 illustrate the achievable SER for indicative spectral efficiencies of $\eta = 6\,\mathrm{bpcu}$ and $\eta = 8\,\mathrm{bpcu}$, respectively. In addition, the effect of varying the d_{TX} distance between the transmitters on the x-axis and y-axis is quantified. This reveals that the proposed APQ-SM modulation scheme appears to be more robust in terms of the separation between the transmitting LEDs for both values of spectral efficiency. Furthermore, as the separation between the LEDs decreases, the achieved SER for the proposed modulation scheme is improved compared to the SM with PAM counterpart. Therefore, it is evident that APQ-SM exhibits an overall enhancement on the achievable SER performance, particularly for higher spectral efficiency values. This can be justified by the fact that for a fixed number of LEDs in the considered room, SM-PAM requires higher order PAM symbols to achieve the same spectral efficiency that is achieved by the proposed APQ-SM scheme.

In the same context, Fig. 5 and Fig. 6 illustrate the SER comparison between the proposed APQ-SM scheme and the MA-SM counterpart for indicative spectral efficiencies of $\eta = 6\,\mathrm{bpcu}$ and $\eta = 8\,\mathrm{bpcu}$, respectively. To that end, it is observed that since the LEDs combinations are used to transmit more information, MA-SM exhibits better performance compared to the SM-PAM, where a single LED is activated. Nevertheless, it is also evident that the proposed APQ-SM scheme exhibits better performance for small LEDs separation, for the case of both considered spectral efficiencies. Therefore, it is overall concluded that the proposed APQ-SM scheme is more robust to the separation distance of the LEDs.

In order to demonstrate the effectiveness of the proposed scheme, we have provided a comparison with the recent work

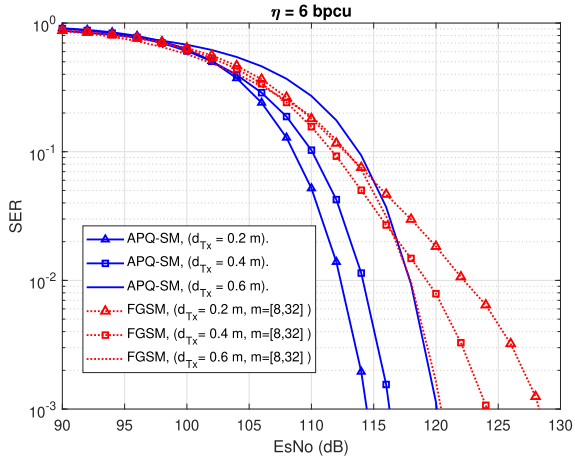

Fig. 7. Comparison between the proposed scheme and FGSM in [7] for spectral efficiency 6 bpcu.

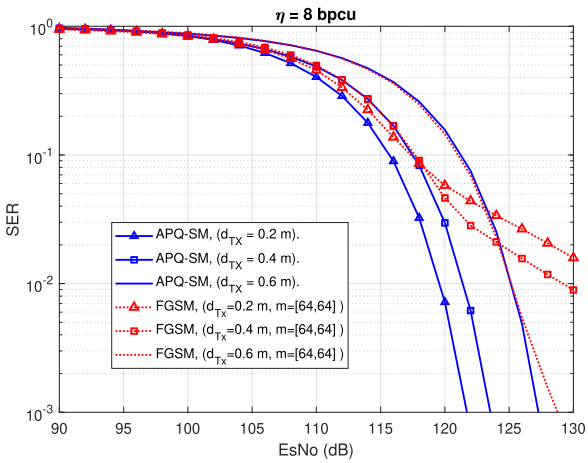

Fig. 8. Comparison between the proposed scheme and FGSM in [7] for spectral efficiency 8 bpcu.

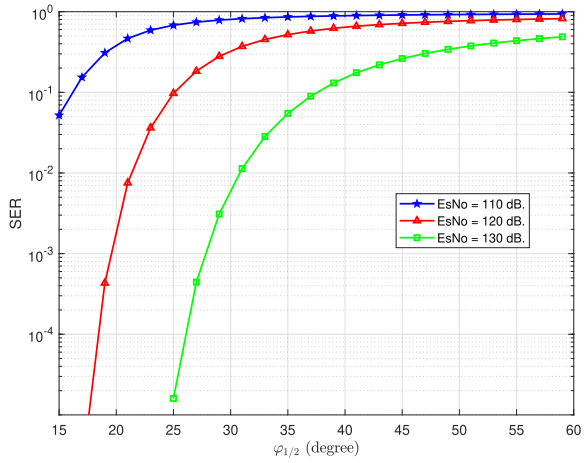

Fig. 9. Effect of the semi-angle at half power on the performance of APQ-SM.

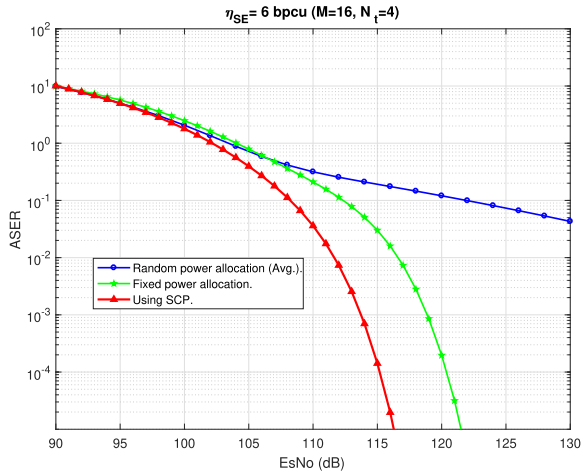

Fig. 10. Comparison between the performance of the APQ-SM with random, fixed, and optimized power allocations for $\eta = 6\,\mathrm{bpcu}$.

on flexible generalized SM (FGSM) in [7]. For fairness, we have considered two fixed spectral efficiency values, i.e., 6 bpcu and 8 bpcu, as depicted in Figs. 7-8, respectively. Furthermore, we assumed that the two schemes work under the same 4×4 MIMO system configuration. For the FGSM, the spectral efficiency of 6 bpcu is achieved by considering two groups of LEDs, where the PAM constellation for the groups are chosen as $m = [8, 32]$ and activating two LEDs to transmit the same PAM symbol. On the other hand, the spectral efficiency of 8 bpcu is achieved by choosing the PAM constellation for the groups as $m = [64, 64]$ and activating two LEDs to transmit the same PAM symbol. It is evident that APQ-SM exhibits an overall enhancement on the achievable SER performance, particularly for higher spectral efficiency values and for correlated MIMO setups. Thus, the proposed scheme is envisioned to provide an improvement on the achievable throughput of SM-based schemes in VLC systems.

Next, we quantify the effect of varying the LED semi-angle on the achievable SER of the considered setup. This variation is considered for different SNR values, as illustrated in Fig. 9. To that end, it is observed that the best SER performance is achieved for low $\varphi_{1/2}$ values. Indeed, a small $\varphi_{1/2}$ leads to an increased Lambertian radiant intensity, which in turn improves the quality of the corresponding communication channel, while reducing the incurred channel correlation. On the contrary, a high $\varphi_{1/2}$ value degrades the quality of the wireless channel, which as a consequence increases the corresponding SER.

Since the power allocation for each part of the APQ symbol is an essential factor that determines the end to end error rate performance of the considered VLC system, we consider the results obtained by solving (P2). Based on this and without loss of generality, we select the following indicative values for the parameters in Algorithm 1: $\alpha_0 = 0.1,\ \alpha_1 = 0.9,\ \alpha_2 = 1,\ \alpha = 1.5,\ \beta = 2,\ \delta^{(0)} = 4,\ \epsilon = 10^{-3}$, and $N_{\max} = 100$ [45]. To this end, we compare the achievable ASER performance under random, fixed and SCP-optimized power allocation factors. Fig. 10 and Fig. 11 demonstrate the ASER for the indicative case of $\eta = 6\,\mathrm{bpcu}$ and $\eta = 8\,\mathrm{bpcu}$, respectively. It becomes evident that random power allocation exhibits the worst achievable ASER performance. On the contrary, the optimum power allocation provides the best performance compared to the random and fixed power allocation approaches. Finally, we investigate

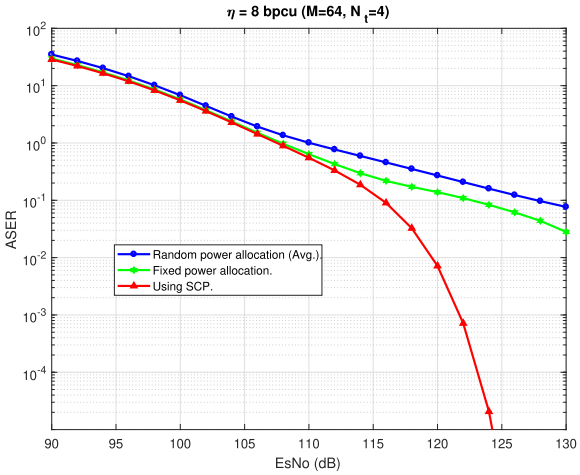

Fig. 11. Comparison between the performance of the APQ-SM with random, fixed, and optimized power allocations for $\eta = 8\,\mathrm{bpcu}$.

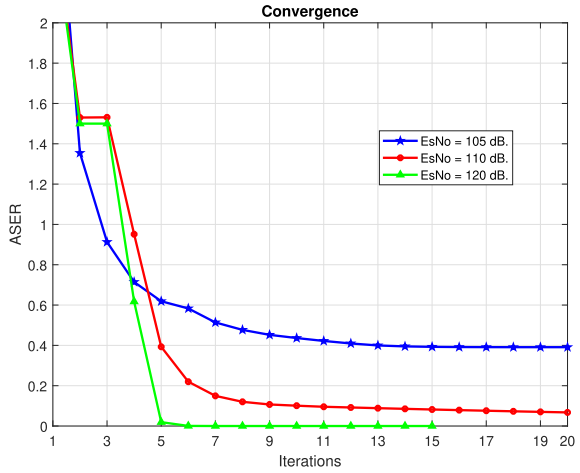

Fig. 12. The convergence behaviour of Algorithm 1.

in Fig. 12 the iteration convergence behavior of Algorithm 1 in terms of the achieved ASER for different SNR values. It is noticed that for higher SNR values, the algorithm converges to the best performance after approximately 5 iterations. This is because increasing the SNR values limits the optimization search space, which in turn provides a faster result. In contrast, the algorithm converges after almost 13 iterations in the case of lower SNR values.

V. Conclusion

This work proposed an effective spatial modulation based scheme, referred to as APQ-SM, which enhances the performance of VLC systems. The proposed scheme transmits information in both the spatial and signal domains in order to increase the achievable spectral efficiency compared to related existing modulation schemes. In addition, the proposed scheme allows the transmission of higher order complex symbols by splitting the signal domain information into three different parts namely, amplitude, phase, and quadrant. Subsequently, each part was modulated using M_i-ary PAM modulation and then all parts were multiplexed in power domain and were transmitted from the active LED utilizing the entire available bandwidth. In this context, an explicit analytic expression was derived for the corresponding ASER of the proposed scheme using both joint and proposed two-step detection methods. It was shown that the proposed scheme is robust to the separation distance between the transmitting LEDs, whilst it achieves better ASER performance at low LEDs separations compared to traditional SM-PAM and MA-SM. Furthermore, the offered analytic and respective simulation results revealed that the corresponding union bound can be considered as a tight upper bound on the exact ASER, from moderate to high SNR values. Finally, in order to demonstrate the effect of the power allocation optimization, we formulated an optimization problem aiming to minimize the ASER. The corresponding presented results showed that optimized power allocation factors yield a significantly improved ASER performance in comparison with random and fixed power counterpart allocation schemes.

References

[1] S. Aboagye, T. M. N. Ngatched, O. A. Dobre, and A. Ibrahim, "Joint access point assignment and power allocation in multi-tier hybrid RF/VLC HetNets," *IEEE Trans. Wireless Commun.*, vol. 20, no. 10, pp. 6329–6342, Oct. 2021.

[2] S. Naser *et al.*, "Rate-splitting multiple access: Unifying NOMA and SDMA in MISO VLC channels," *IEEE Open J. Veh. Technol.*, vol. 1, pp. 393–413, 2020, doi: 10.1109/OJVT.2020.3031656.

[3] A. Ijaz, M. M. U. Rahman, and O. A. Dobre, "On safeguarding visible light communication systems against attacks by active adversaries," *IEEE Photon. Technol. Lett.*, vol. 32, no. 1, pp. 11–14, Jan. 2020.

[4] A. M. Aljaberi, S. A. Naser, P. C. Sofotasios, and S. Muhaidat, "Space shift keying modulation in non-orthogonal multiple access hybrid visible light communication systems," in *Proc. 3rd Int. Conf. Adv. Commun. Technol. Netw.*, 2020, pp. 1–5.

[5] Y. Xiao and Y.-J. Zhu, "Chromaticity-adaptive generalized spatial modulation for MIMO VLC with multi-color LEDs," *IEEE Photon. J.*, vol. 11, no. 4, Aug. 2019, Art. no. 7904112.

[6] S. Aboagye, T. M. N. Ngatched, O. A. Dobre, and A. R. Ndjiongue, "Intelligent reflecting surface-aided indoor visible light communication systems," *IEEE Commun. Lett.*, vol. 25, no. 12, pp. 3913–3917, Dec. 2021.

[7] M. Al-Nahhal, E. Basar, and M. Uysal, "Flexible generalized spatial modulation for visible light communications," *IEEE Trans. Veh. Technol.*, vol. 70, no. 1, pp. 1041–1045, Jan. 2021.

[8] S. A. Naser and P. C. Sofotasios, "Generalization of space-time block coded-spatial modulation for high data rate VLC systems (*invited paper*)," in *Proc. 3rd Int. Conf. Adv. Commun. Technol. Netw.*, 2020, pp. 1–5.

[9] H. Abumarshoud, L. Mohjazi, and S. Muhaidat, "Amplitude, phase, and quadrant (APQ) modulation for indoor visible light communications," *Phys. Commun.*, vol. 48, Oct. 2021, Art. no. 101440.

[10] Z. Zheng, H. Du, J. Xue, and Z. Wu, "Adaptive spatial modulation for indoor visible light communications," *IEEE Commun. Lett.*, vol. 24, no. 10, pp. 2240–2244, Oct. 2020.

[11] X. Cheng, M. Zhang, M. Wen, and L. Yang, "Index modulation for 5 G: Striving to do more with less," *IEEE Wireless Commun.*, vol. 25, no. 2, pp. 126–132, Apr. 2018.

[12] F. Wang *et al.*, "Secrecy analysis of generalized space-shift keying aided visible light communication," *IEEE Access*, vol. 6, pp. 18310–18324, Jan. 2018.

[13] N. Su, E. Panayirci, M. Koca, A. Yesilkaya, H. Vincent Poor, and H. Haas, "Physical layer security for multi-user MIMO visible light communication systems with generalized space shift keying," *IEEE Trans. Commun.*, vol. 69, no. 4, pp. 2585–2598, Apr. 2021.

[14] R. Mesleh, H. Haas, C. W. Ahn, and S. Yun, "Spatial modulation a new low complexity spectral efficiency enhancing technique," in *Proc. 1st Int. Conf. Commun. Netw. China*, 2006, pp. 1–5.

[15] M. L. Tran and S. Kim, "Receiver-oriented spatial modulation in visible light communication system," *IEEE Access*, vol. 7, pp. 129666–129677, Sep. 2019.

[16] X. Gao, Z. Bai, P. Gong, and D. O. Wu, "Design and performance analysis of LED-grouping based spatial modulation in the visible light communication system," *IEEE Trans. Veh. Technol.*, vol. 69, no. 7, pp. 7317–7324, Jul. 2020.

[17] C. R. Kumar and R. K. Jeyachitra, "Power efficient generalized spatial modulation MIMO for indoor visible light communications," *IEEE Photon. Technol. Lett.*, vol. 29, no. 11, pp. 921–924, Jun. 2017.

[18] C. R. Kumar and R. K. Jeyachitra, "Dual-mode generalized spatial modulation MIMO for visible light communications," *IEEE Commun. Lett.*, vol. 22, no. 2, pp. 280–283, Feb. 2018.

[19] M. H. Khadr, I. Walter, H. Elgala, and S. Muhaidat, "Machine learning-based massive augmented spatial modulation (ASM) for IoT VLC systems," *IEEE Wireless Commun. Lett.*, vol. 25, no. 2, pp. 494–498, Feb. 2021.

[20] S. B. Cihan, E. Başar, and E. Panaylrcl, "Optical spatial modulation ofdm system design," in *Proc. 24th Signal Process. Commun. Application Conf.*, 2016, pp. 1073–1076.

[21] K. Xu, H. Yu, and Y.-J. Zhu, "Channel-adapted spatial modulation for massive MIMO visible light communications," *IEEE Photon. Technol. Lett.*, vol. 28, no. 23, pp. 2693–2696, Dec. 2016.

[22] J.-Y. Wang, H. Ge, J.-X. Zhu, J.-B. Wang, J. Dai, and M. Lin, "Adaptive spatial modulation for visible light communications with an arbitrary number of transmitters," *IEEE Access*, vol. 6, pp. 37 108–37 123, 2018.

[23] J.-Y. Wang, J.-X. Zhu, S.-H. Lin, and J.-B. Wang, "Adaptive spatial modulation based visible light communications: SER analysis and optimization," *IEEE Photon. J.*, vol. 10, no. 3, Jun. 2018, Art. no. 7903814.

[24] R. Tejaswi, T. L. Narasimhan, and A. Chockalingam, "Quad-LED complex modulation (QCM) for visible light wireless communication," in *Proc. IEEE Wireless Commun. Netw. Conf. Workshops*, 2016, pp. 18–23.

[25] Q. Zhang, Z. Bai, N. Zhang, S. Sun, T. Han, and K. S. Kwak, "Performance analysis of quad-LED complex spatial modulation in visible light communication system," in *Proc. IEEE Wireless Commun. Netw. Conf.*, 2018, pp. 1–5.

[26] K. V. S. S. Sushanth and A. Chockalingam, "Multiple-LED complex modulation schemes for indoor MIMO VLC systems," in *Proc. IEEE Int. Conf. Commun.*, 2019, pp. 1–6.

[27] Z. Ghassemlooy, W. Popoola, and S. Rajbhandari, *Optical Wireless Communications: System and Channel Modelling With MATLAB*, 2nd ed. Boca Raton, FL, USA: CRC Press, 2019.

[28] T. Komine and M. Nakagawa, "Fundamental analysis for visible-light communication system using LED lights," *IEEE Trans. Consum. Electron.*, vol. 50, no. 1, pp. 100–107, Feb. 2004.

[29] R. Mesleh, H. Elgala, and H. Haas, "On the performance of different OFDM based optical wireless communication systems," *IEEE/OSA J. Opt. Commun. Netw.*, vol. 3, no. 8, pp. 620–628, Aug. 2011.

[30] A. Prudnikov, Y. Brychkov, I. Brychkov, and O. Marichev, *Integrals and Series*, vol. 2, *Special Functions* (Tranls. N. M. Queen). Amsterdam, The Netherlands: Gordon and Breach Science Publishers, 1986.

[31] Y. Mao, B. Clerckx, and V. O. K. Li, "Energy efficiency of rate-splitting multiple access, and performance benefits over SDMA and NOMA," in *Proc. 15th Int. Symp. Wireless Commun. Syst.*, 2018, pp. 1–5.

[32] L. Sampath, B. V. Patil, H. Gooi, J. Maciejowski, and K. Ling, "A trust-region based sequential linear programming approach for AC optimal power flow problems," *Electric Power Syst. Res.*, vol. 165, pp. 134–143, 2018.

[33] W. Sheng, K. Liu, S. Cheng, X. Meng, and W. Dai, "A trust region SQP method for coordinated voltage control in smart distribution grid," *IEEE Trans. Smart Grid*, vol. 7, no. 1, pp. 381–391, Jan. 2016.

[34] Y. Mao, M. Szmuk, and B. Açlkmeşe, "Successive convexification of non-convex optimal control problems and its convergence properties," in *Proc. IEEE 55th Conf. Decis. Control*, 2016, pp. 3636–3641.

[35] M. S. Lobo, L. Vandenberghe, S. Boyd, and H. Lebret, "Applications of second-order cone programming," *Linear Alg. Appl.*, vol. 284, no. 1, pp. 193–228, Nov. 1998.

[36] W. Jaafar, S. Naser, S. Muhaidat, P. C. Sofotasios, and H. Yanikomeroglu, "On the downlink performance of RSMA-based UAV communications," *IEEE Trans. Veh. Technol.*, vol. 69, no. 12, pp. 16 258–16 263, Dec. 2020.

[37] S. Boyd and L. Vandenberghe, *Convex Optimization*. New York, NY, USA: Cambridge Univ. Press, 2004.

[38] T. Fath and H. Haas, "Performance comparison of MIMO techniques for optical wireless communications in indoor environments," *IEEE Trans. Commun.*, vol. 61, no. 2, pp. 733–742, Feb. 2013.

[39] T. Fath and H. Haas, "Optical spatial modulation using colour LEDs," in *Proc. IEEE Int. Conf. Commun.*, 2013, pp. 3938–3942.

[40] C. He, T. Q. ang, and J. Armstrong, "Performance of optical receivers using photodetectors with different fields of view in a MIMO ACO-OFDM system," *J. Lightw. Technol.*, vol. 33, no. 23, pp. 4957–4967, Dec. 2015.

[41] C. He, T. Q. Wang, M. Abdullah Masum, and J. Armstrong, "Performance of optical receivers using photodetectors with different fields of view in an indoor cellular communication system," in *Proc. Int. Telecommun. Netw. Appl. Conf.*, 2015, pp. 77–82.

[42] L. Yin, W. O. Popoola, X. Wu, and H. Haas, "Performance evaluation of non-orthogonal multiple access in visible light communication," *IEEE Trans. Commun.*, vol. 64, no. 12, pp. 5162–5175, Dec. 2016.

[43] A. Stavridis and H. Haas, "Performance evaluation of space modulation techniques in VLC systems," in *Proc. IEEE Int. Conf. Commun. Workshop*, 2015, pp. 1356–1361.

[44] S. P. Alaka, T. L. Narasimhan, and A. Chockalingam, "Generalized spatial modulation in indoor wireless visible light communication," in *Proc. IEEE Glob. Commun. Conf.*, 2015, pp. 1–7.

[45] J. Nocedal and S. J. Wright, "Trust-region methods," in *Numerical Optimization*. ser. Springer Series in Operations Research and Financial Engineering. New York, NY, USA: Springer, New York, NY, 2006, pp. 66–100.